Achieving High Exciton Utilization with Folded π-Molecules

Shidang Xu
National University of Singapore
Bin Liu (cheliub@nus.edu.sg)
National University of Singapore https://orcid.org/0000-0002-0956-2777

Article

Keywords: folded π-Molecules, high exciton utilization, solids

Posted Date: March 19th, 2021

DOI: https://doi.org/10.21203/rs.3.rs-318062/v1

Abstract

π-Molecules play important roles in many applications such as organic light emitting devices, photocatalysis, photovoltaics, biosensors and medicine. Very often, high-performance π-conjugated molecules are of great research interest. However, owing to the conflict between the design of efficient π structure (good rigidity and planarity) and efficient π aggregates (minimum face-to-face π effect), it is challenging for traditional planar π or recently emerged twisted π molecules to realize very high exciton utilization in solid state. Herein, we report a new π skeleton, folded π, to achieve high exciton utilization in solids. Folded π-based molecules tend to form molecular packing patterns that are rich in π interactions, favoring the suppression of unfavorable energy dissipation pathways such as molecular thermal perturbation. Meanwhile, the potential face-to-face π effect between planar π is well prevented by the hydrogen atoms around the π planes. As a result of effective packing, all the synthesized π-based molecules show very high exciton utilization in solids.

Introduction

π-Based molecules are one type of the most common organic molecules in materials science, which have been widely used in organic light-emitting diodes[1-2], photocatalysis[3], organic field-effect transistors[4-5], photovoltaics[6-7], sensors[8], and biomedical applications[9-10]. For most of the applications, high quantum yield plays a very important role, which reflects the effective utilization of excited state[11-13].

A known theory on improving excited state utilization is the minimization of molecular thermal perturbation (or intramolecular motion)[14-16], which is the major unfavorable energy dissipation pathway that consumes exciton. Representative strategies include designing rigid molecular skeleton, isotope substitution of hydrogen and designing tight molecular packing[14]. With improved understanding of excited-state species (especially exciton of different spin state), in recent decades, a few molecular strategies emerged based on the full or even “excessive” utilization of excitons, such as triplet utilization via reverse intersystem crossing (RISC) [17-18], and exciton doubling by singlet fission[19-20]. In order to achieve high exciton utilization, suppressing unwanted energy dissipation pathways and increasing available excitons are both essential. However, for π-based molecules, one conflict is that efficient π skeleton (good rigidity and planarity and thus less thermal perturbation) is likely to yield strong face-to-face π-π interaction that causes exciton quenching[21-22]. A direct solution is to add spacers to the molecules, which however, may dilute the optically active component and make the material processing difficult. The other solution is to compromise molecular rigidity and design non-planar π structure, e.g. twisted π structure or rotor structure[23], which effectively prevents the π-π effect. Though with poor molecular rigidity, in some cases, non-planar π molecules pack in the way that molecular motion is well locked by intermolecular interactions, resulting in organic solids with high quantum yields close to unity[24-26]. However, in most cases, the exciton utilization is unsatisfactory[13,26].

To develop efficient π based molecules/systems, we herein report a folded π molecular skeleton, which is consisted of 2-3 folding π planes (Scheme 1). Compared with traditional π skeletons, folded-π skeleton is less likely to bring in strong face-to-face π-π interaction, but more likely to form effective packing for high exciton utilization. We designed and synthesized a series of folded π molecules which can be classified into three categories, namely 2π (compounds **1-8**, consist of two π planes), 3π-trans and 3π-cis (compounds **9-10** and **11-12**, comprised of three π planes with two side planes folding in the opposite or same orientation, respectively). All the designed folded π molecules are able to form well-regulated packing patterns for high exciton utilization: high packing level with intramolecular motion well restricted by abundant weak π interactions. As a result, all the synthesized folded π molecules show high quantum yields close to unity.

Results

Design of folded π molecules. Owing to their specific conformation, folded-π molecules are less prone to form strong face-to-face π-π interactions as compared with planar π system. Figure 1 shows the energy surface of two π molecules versus intermolecular distance. When the folded angle (Θ) is less than 120-130 degree, it is less likely for two π systems to get close enough to form π-π interaction, which generally demands the interplane distance to be less than 3.8 angstroms. The relatively large intermolecular distance for folded π structures could be due to the steric effect of hydrogens around the π planes. Instead of forming π-π interaction, the π planes of folded π will form abundant weak π interactions (e.g. CH…π). On the other hand, folded π is more prone to form tight packing in comparison with twisted π structure. Owing to the building block-liked shape, folded π structure will form particular packing patterns including “box”, “braid” and “stairs” (Figure 2). All these patterns are tight packing modes with high packing level and the intramolecular motions will be well locked by abundant weak π interactions. In contrast, the packing of twisted-π structures is unpredictable and the chance to form high-level packing is not high.

The key to designing a folded-π structure with Θ < 130 is the conformation of the bridging atom of the π planes (Figure 2b, X, e.g. C, Si, N, P). For example, in an aryl-aryl system, sp^3 and sp^2 hybridization of the bridging atom leads to two different conformations of the π system (Figure 2b). In this case, sp^3 hybridization of the bridging atom is the key of folding conformation. To form a stable sp^3 X in such a π system, the lone pair of X atom should have a high tendency to be conjugated with the adjacent π plane, such as an electron-poor π with strong electron-withdrawing groups (A, e.g. cyano group). The stronger the electron-withdrawing group, the higher tendency for the X atom to be sp^3 hybridized (Figure 2b).

Achieving high exciton utilization with 2π molecules. According to the “building block” formula, we first designed and synthesized compounds **1-8** with two folded π planes (2π). The synthesis and structural characterization of **1-8** are described in the supporting information. All eight compounds were obtained with good purity and their single crystals were obtained by slow evaporation from proper solvents (e.g. chloroform, acetone), after which single-crystal X-ray diffraction studies were conducted. From the single-crystal structures, the 2π folded-π structures are found to pack in particular patterns (“box”, “braid” and

“stair”, Figure 2). For “box” pattern, the primary intermolecular interaction is between the side and face of two π planes, which specifically are CH•••π and n•••π for **1**-**4** (Figure 3a). The unique double side-to-face interactions of π planes in a symmetric way lead to abundance of π effects with a total interaction number of 20, 26, 18 and 23 per molecule for **1-4,** respectively (Figure S35). The total number of interactions per molecule for **1-4** is much more than those representative solid-state π systems such as 6 for tetraphenylethene, and 4 each for tetraphenylpyran or distyreneanthrancene or triphenylamine (Supporting information, Figure S39). Though without significant π effect, the numerous weak π interactions lead to high packing energy of -318.5, -288.3, -257.8 and -273.7 kJ/mol per molecule for **1-4**, respectively. We also calculated the packing energy of a series of classic twisted-π systems (Table S1) using the same method. It was found that the packing energy of **1-4** is much higher than those representative twisted-π systems.

Next, we investigated the exciton utilization of the “box” by measuring their photoluminescence quantum yields (PLQY) and single oxygen quantum yields (SOQY). As photoluminescence and singlet oxygen generation are competing pathways, their sum reflects the experimental utilization of excitons. As expected from the effective packings, **1-4** show high exciton utilization with total quantum yields of 0.72, 0.99, 0.89 and 0.83, respectively (Figure 3c).

For “braid“ and “stair“ patterns, the major intermolecular interaction is between side and face (one-way) as well, and sometimes involves weak face-to-face contact of the π planes. Owing to the steric effect of the numerous hydrogens around the side of the π planes, 2π molecule is less likely to form close face-to-face π interaction in “braid“ and “stair“ patterns. Similar to “box“, the unique “braid“ and “stair“ patterns lead to abundant π effects with a total interaction number of 15, 17, 19 and 18 per molecule for **5-8**, respectively (Figure S36). The numerous weak π interactions account for high total packing energy of -212.2, -207.2, -217.5 and -218.9 kJ/mol per molecule for **5-8**, respectively. We then investigated the exciton utilization of **5-8** by measuring their PLQYand SOQY. As expected from the effective packings, **5-8** show high exciton utilization with add-up quantum yields of 0.93, 0.77, 0.92 and 0.71, respectively (Figure 4c).

Achieving high exciton utilization with 3π molecules. The “folded π” formula was also utilized for the design and synthesis of **“3π” folded-π structures** (**9-10**). Figure 5a shows the crystalline structures of compounds **9-10**. They have similar “3π-trans” conformation. From the single-crystal structures, we found “3π-trans” folded-π molecules tend to pack in “stair” pattern (Figure 5a), which is the only packing pattern for such a “building block”. Similar to 2π molecules, the hydrogens around π planes effectively prevent strong face-to-face π effect. Meanwhile, the unique 3π-trans conformation allows molecules to pack tightly with abundant π interactions. The primary interactions for **9-10** are CH•••π, n•••π and CH•••O, which contribute to total interaction numbers of 20 and 30 per molecule for **9** and **10**, respectively (Figure S37). As a result of high packing level, the packing energy of **9** and **10** are -283.9 and -288.6 kJ/mol per molecule, respectively (Figure 5c). We also measured the PLQY and SOQY for compounds **9** and **10** and as expected, they both show high total quantum yields of 0.99 and 0.93, respectively. Figure 5a shows the crystalline structures of compounds **11** and **12**, which possess similar “3π-cis” conformation. It is

found that both **11** and **12** pack in unique double “box” pattern (box-*db*)—one molecule forms double side-to-face with two other 3π-cis molecules, leading to artful molecular necklaces. The unique packing modes of **11** and **12** also lead to abundant π effects with a total interaction numbers of 20 and 22 per molecule (Figure S38) and high packing energy of 349.0 and -277.8 kJ/mol for **11** and **12**, respectively. As a result of effective packing, the total quantum yield for **11** and **12** reaches 0.74 and 0.78, respectively.

Summary

Herein we introduced a new π skeleton for the development of π-based materials with high exciton utilization in solid state. The folded-π molecular design solves the conflict between efficient π structure and effective π packing, showing high potential for future π design. In these new π systems, a series of organic solids with high quantum yields of close to unity were obtained. Basing on the folded π skeleton, excellent solid-state properties become highly achievable, in combination with a wise choice of π motif. We believe folded π design will offer new opportunities to design high performance solid-state emitters for different research fields, such as room-temperature phosphorescence, organic afterglow, and mechano-luminescence.

Methods

General

All starting materials are commercially available and were used as supplied unless otherwise indicated. All experiments were conducted in air unless otherwise noted. 4-Bromobenzonitrile, 2,3-bis(4-bromophenyl)fumaronitrile, bis(4-fluorophenyl)methanone, 2-bromoanthracene-9,10-dione, 2-(4-bromophenyl)-4,6-diphenyl-1,3,5-triazine, 1-methylphenothiazine, dibromobenzophenone, 2,8-dibromodibenzothiophene, 2-bromo-9H-thioxanthen-9-one 10,10-dioxide, malononitrile, 4-bromoiodobenzene, and other chemicals and reagents for the synthesis were purchased from Sigma-Aldrich and Tee Hai Chem Ltd., and used as received without any further purification. Compound **1-12** and related intermediates were synthesized and characterized according to the methods described in section SI.

NMR spectra were recorded on a Bruker ARX 400 NMR spectrometer. Chemical shifts are recorded in parts per million referenced according to residual solvent ($CDCl_3$ = 7.26 ppm) in ^{1}H NMR and ($CDCl_3$ = 77.0 ppm) in ^{13}C NMR. Mass spectra were reported on the AmaZon X LC-MS for ESI. X-ray crystallography was carried out on a Bruker D8 Venture Kappa four circles X-ray Diffractometer with a Photon II CPAD Detector. Data were collected at 100K using an Oxford Cryostream 800 Cooler. Bruker Apex 3 program was used to calculate total number of images for 100% completeness up to resolution of 0.75 Å for Mo radiation. Data were measured using omega and phi scans of 0.5° per frame. A cell parameters were obtained by Apex 3 program. UV-vis absorption spectra were obtained on a Shimadzu Model UV-1700

spectrometer. Photoluminescence (PL) spectra were measured on a Perkin-Elmer LS 55 spectrofluorometer. All UV and PL spectra were collected at 24 ± 1 °C.

Fabrication of nanocrystals and measurement of quantum yields

Nanocrystal samples **1-12** were prepared directly from the corresponding solid crystals using a top-down approach. A bulk crystal (1 mg) was added to the aqueous solution of 1,2-distearoyl-*sn*-glycero-3-phosphoethanolamine-N-[maleimide(polyethylene glycol)-2000] (DSPE-PEG_{2000}-Mal) (4 mg/mL, 10 mL) under continuous sonication with a microtip-equipped probe sonicator for 20 min. Next, the aqueous suspension was filtered through a 0.22 μm PTFE syringe-driven filter (Millipore) and eventually, a clear nanocrystal suspension was obtained. PLQYs of the samples were measured using quinine sulfate, Rhodamine 6G and 4-(dicyanomethylene)-2-methyl-6-(4-dimethylaminostyryl)-4H-pyran as the standards. The singlet oxygen generation efficiencies of the samples were subsequently tested under white light (400-700 nm, 250 mW/cm^2) irradiation, using 9,10-anthracenediyl-bis(methylene)dimalonic acid as an indicator.

Computational Details

The potential energy surface for molecular dimer shown in Figure 1 with differenty folded angle is calculated by using a M062X/6-31* method. The potential energy surface is scanned with intermolecular distance ranging from 2.2 to 6.7 Å (step: 0.15 Å). The excited-state characteristics were calculated by the time-dependent density functional theory (TD-DFT) using single crystal structure geometries.

Declarations

CCDC 1555301, 1041212, 948737, 1847298, 1040892, 1426128, 1421265, 1527590 and 1846159 contain the crystallographic data for this paper. These data can be obtained free of charge from The Cambridge Crystallographic Data Centre.

Acknowledgement

The authors thank the Singapore National Research Foundation (R279-000-444-281 and R279-000-483-281), and the National University of Singapore (R279-000-482-133) for financial support.

Author Contribution

S.X. devised and performed all the modelling and experiments. B.L. supervised the project. S.X. and B.L. discussed the results and edited the manuscript.

Competing financial interests

The authors declare no competing financial interests.

References

1. D. Di, A. S. Romanov, L. Yang, J. M. Richter, J. P. H. Rivett, S. Jones, T. H. Thomas, M. Abdi Jalebi, R. H. Friend, M. Linnolahti, M. Bochmann, D. Credgington, High-performance light-emitting diodes based on carbene-metal-amides. *Science* **356**, 159-163 (2017).
2. H. Uoyama, K. Goushi, K. Shizu, H. Nomura, C. Adachi, Highly efficient organic light-emitting diodes from delayed fluorescence. *Nature* **492**, 234-+ (2012).
3. I. Ghosh, J. Khamrai, A. Savateev, N. Shlapakov, M. Antonietti, B. König, Organic semiconductor photocatalyst can bifunctionalize arenes and heteroarenes. *Science* **365**, 360-366 (2019).
4. X. G. Guo, A. Facchetti, T. J. Marks, Imide- and Amide-Functionalized Polymer Semiconductors. *Chem. Rev.* **114**, 8943-9021 (2014).
5. D. Zhao, J. Chen, B. Wang, G. Wang, Z. Chen, J. Yu, X. Guo, W. Huang, T. J. Marks, A. Facchetti, Engineering Intrinsic Flexibility in Polycrystalline Molecular Semiconductor Films by Grain Boundary Plasticization. *J. Am. Chem.Soc.* **142**, 5487-5492 (2020).
6. X. G. Guo, N. J. Zhou, S. J. Lou, J. Smith, D. B. Tice, J. W. Hennek, R. P. Ortiz, J. T. L. Navarrete, S. Y. Li, J. Strzalka, L. X. Chen, R. P. H. Chang, A. Facchetti, T. J. Marks, Polymer solar cells with enhanced fill factors. *Nat. Photon.* **7**, 825-833 (2013).
7. L. X. Meng, Y. M. Zhang, X. J. Wan, C. X. Li, X. Zhang, Y. B. Wang, X. Ke, Z. Xiao, L. M. Ding, R. X. Xia, H. L. Yip, Y. Cao, Y. S. Chen, Organic and solution-processed tandem solar cells with 17.3% efficiency. *Science* **361**, 1094-+ (2018).
8. A. G. Beyene, K. Delevich, J. T. Del Bonis-O'Donnell, D. J. Piekarski, W. C. Lin, A. W. Thomas, S. J. Yang, P. Kosillo, D. Yang, G. S. Prounis, L. Wilbrecht, M. P. Landry, Imaging striatal dopamine release using a nongenetically encoded near infrared fluorescent catecholamine nanosensor. *Sci. Adv.* **5**, eaaw3108 (2019).
9. A. L. Antaris, H. Chen, K. Cheng, Y. Sun, G. S. Hong, C. R. Qu, S. Diao, Z. X. Deng, X. M. Hu, B. Zhang, X. D. Zhang, O. K. Yaghi, Z. R. Alamparambil, X. C. Hong, Z. Cheng, H. J. Dai, A small-molecule dye for NIR-II imaging. *Nat. Mater.* **15**, 235 (2016).
10. J. Huang, J. Li, Y. Lyu, Q. Miao, K. Pu, Molecular optical imaging probes for early diagnosis of drug-induced acute kidney injury. *Nat. Mater.* **18**, 1133-1143 (2019).
11. J. Jagielski, S. Kumar, M. Wang, D. Scullion, R. Lawrence, Y.-T. Li, S. Yakunin, T. Tian, M. V. Kovalenko, Y.-C. Chiu, E. J. G. Santos, S. Lin, C.-J. Shih, Aggregation-induced emission in lamellar solids of colloidal perovskite quantum wells. *Sci. Adv.* **3**, eaaq0208 (2017).
12. J. Jeon, D. G. You, W. Um, J. Lee, C. H. Kim, S. Shin, S. Kwon, J. H. Park, Chemiluminescence resonance energy transfer–based nanoparticles for quantum yield–enhanced cancer phototheranostics. *Sci. Adv.* **6**, eaaz8400 (2020).
13. Z. Yang, Z. Mao, Z. Xie, Y. Zhang, S. Liu, J. Zhao, J. Xu, Z. Chi, M. P. Aldred, Recent advances in organic thermally activated delayed fluorescence materials. *Chem. Soc. Rev.* **46**, 915-1016 (2017).

14. N. J. Turro, V. Ramamurthy, J. C. Scaiano, Quantum dynamics: Transitions between states, in Principle of Molecular Photochemistry: An Introduction (University Science Books, 2009), chap. 3, pp. 113–118.
15. O. Bolton, K. Lee, H.-J. Kim, K. Y. Lin, J. Kim, Activating efficient phosphorescence from purely organic materials by crystal design. *Nat. Chem.* **3**, 205-210 (2011).
16. M. S. Kwon, Y. Yu, C. Coburn, A. W. Phillips, K. Chung, A. Shanker, J. Jung, G. Kim, K. Pipe, S. R. Forrest, J. H. Youk, J. Gierschner, J. Kim, Suppressing molecular motions for enhanced room-temperature phosphorescence of metal-free organic materials. *Nat. Commun.* **6**, 8947 (2015).
17. T. Hosokai, H. Matsuzaki, H. Nakanotani, K. Tokumaru, T. Tsutsui, A. Furube, K. Nasu, H. Nomura, M. Yahiro, C. Adachi, Evidence and mechanism of efficient thermally activated delayed fluorescence promoted by delocalized excited states. *Science Advances* **3**, e1603282 (2017).
18. H. Noda, H. Nakanotani, C. Adachi, Excited state engineering for efficient reverse intersystem crossing. *Sci. Adv.* **4**, eaao6910 (2018).
19. J. Q. Zhang, H. S. Tan, X. G. Guo, A. Facchetti, H. Yan, Material insights and challenges for non-fullerene organic solar cells based on small molecular acceptors. *Nat. Energy* **3**, 720-731 (2018).
20. M. B. Smith, J. Michl, Singlet Fission. *Chem.Rev.* **110**, 6891-6936 (2010).
21. T. Förster, K. Kasper, Ein Konzentrationsumschlag der Fluoreszenz. *Z. Phys. Chem.* (Muenchen, Ger.) **1**, 275-277 (1954).
22. J. B. Birks, Photophysics of Aromatic Molecules; (Wiley, London, 1970).
23. J. Mei, N. L. C. Leung, R. T. K. Kwok, J. W. Y. Lam, B. Z. Tang, Aggregation-Induced Emission: Together We Shine, United We Soar! *Chem. Rev.* **115**, 11718-11940 (2015).
24. B. Huang, W. C. Chen, Z. Li, J. Zhang, W. Zhao, Y. Feng, B. Z. Tang, C. S. Lee, Manipulation of Molecular Aggregation States to Realize Polymorphism, AIE, MCL, and TADF in a Single Molecule. *Angew. Chem. Int. Ed.* **57**, 12473-12477 (2018).
25. Z. Xie, B. Yang, F. Li, G. Cheng, L. Liu, G. Yang, H. Xu, L. Ye, M. Hanif, S. Liu, D. Ma, Y. Ma, Cross dipole stacking in the crystal of distyrylbenzene derivative: the approach toward high solid-state luminescence efficiency. *J. Am. Chem. Soc.* **127**, 14152-14153 (2005).
26. S. Xu, Y. Duan, B. Liu, Precise Molecular Design for High-Performance Luminogens with Aggregation-Induced Emission. *Adv. Mater.* **32**, 1903530 (2020).

Figures

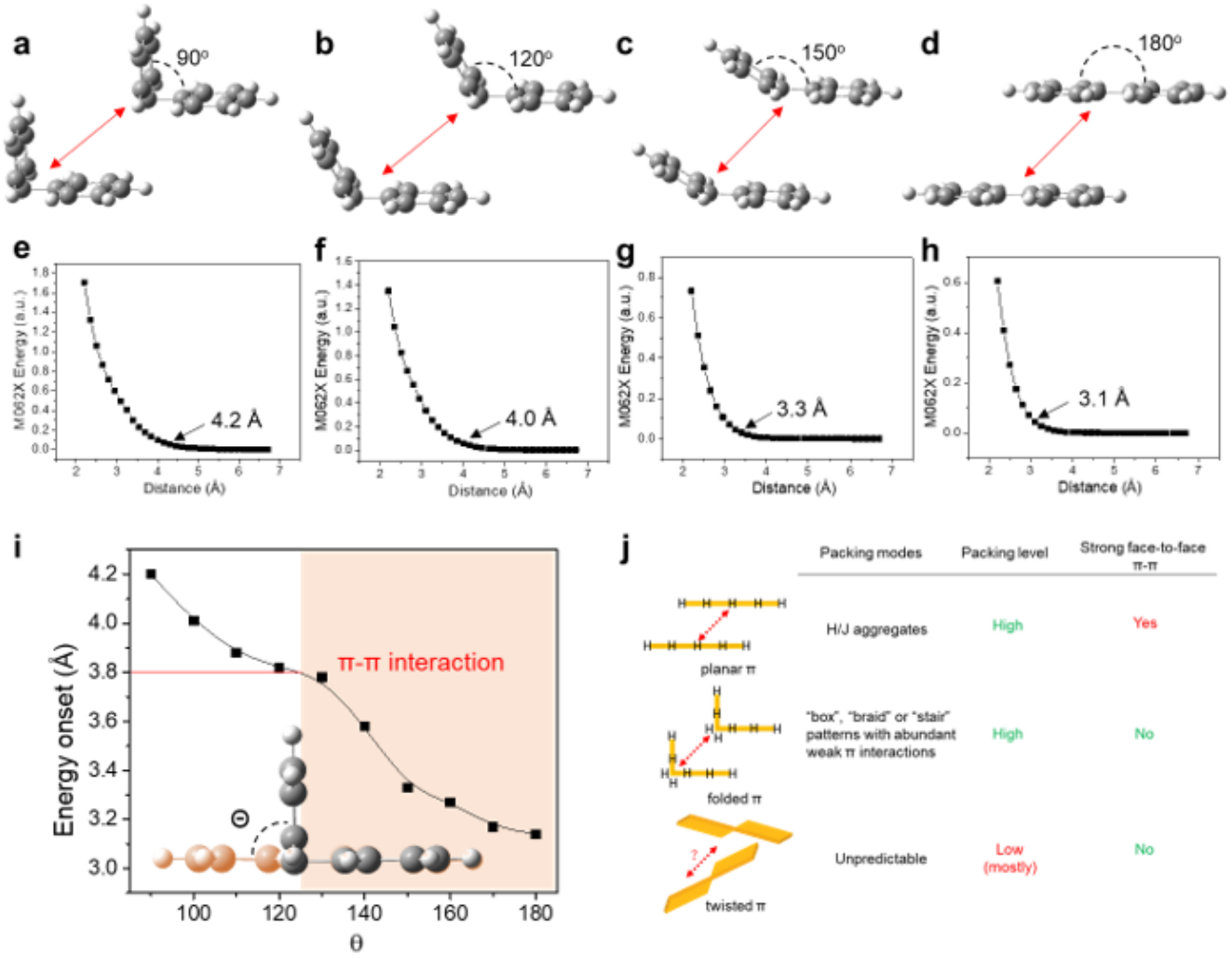

Figure 1

Folded π structure and π-π interaction. (a-d) Molecular dimer of π systems (benzene-benzene) with folded angle of 90, 120, 150 and 180 degree, respectively, and corresponding potential energy surface, intermolecular distance scaning from 2.2 to 6.7 angstroms (e-h). (i) Energy onset of π systems with different foleded angle. (j). Comparison among planar π, folded π and twisted π systems.

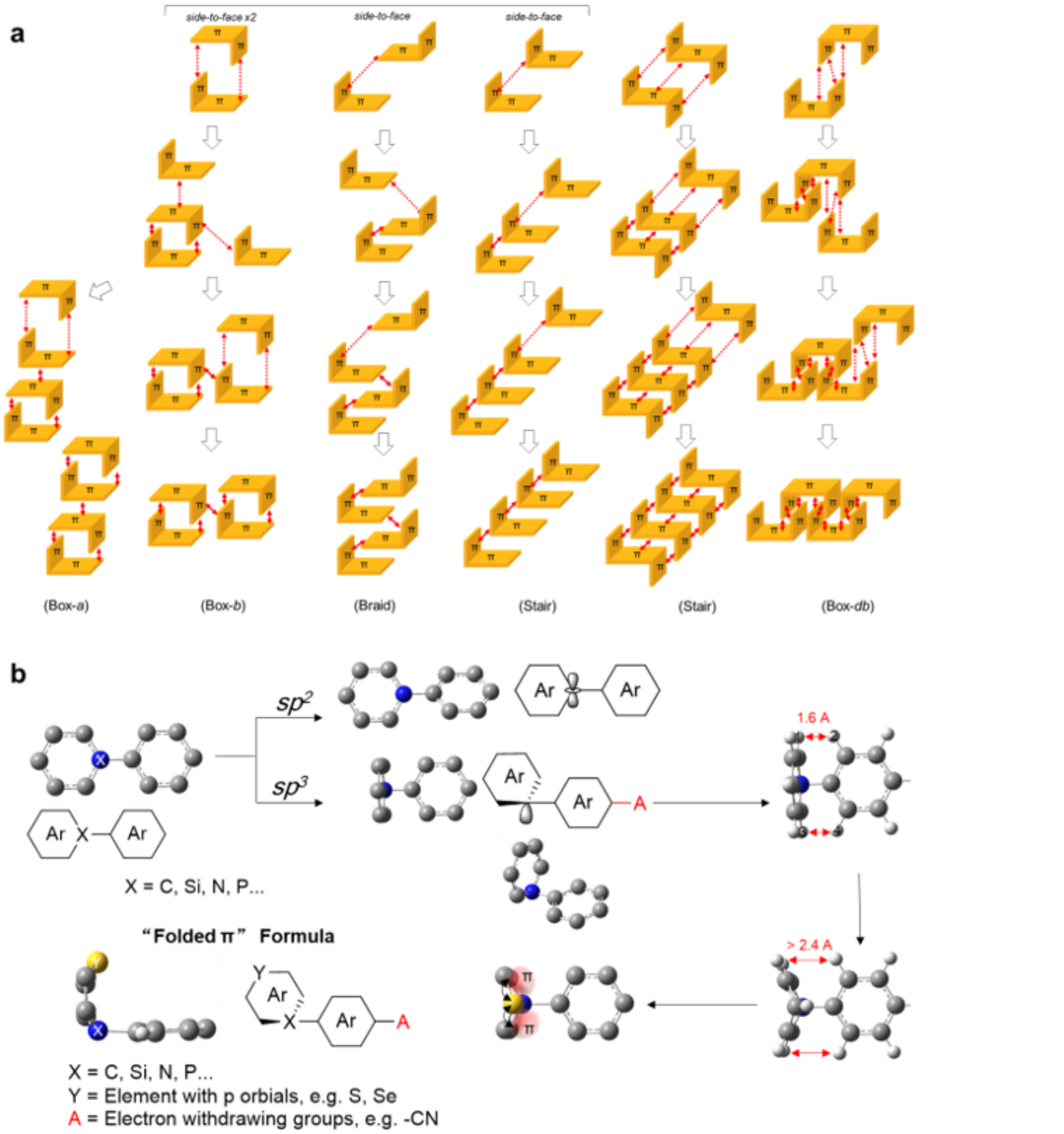

Figure 2

Packing patterns and design formula for folded π molecules. (a) Packing patterns for 2π, 3π-trans and 3π-cis molecules. (b) The conformation of a π system associated with both electron conjugation and steric hindrance. Step 1: Design the connecting atom. To realize a folded π conformation, the connecting atom (X) should be of sp3 hybridization. The candidates of the connecting atom are C, Si, N and P. Step

2: Decrease the steric effect. Step 3: Introducing element with abundant p orbitals to stabilize a boat-shaped aryl structure.

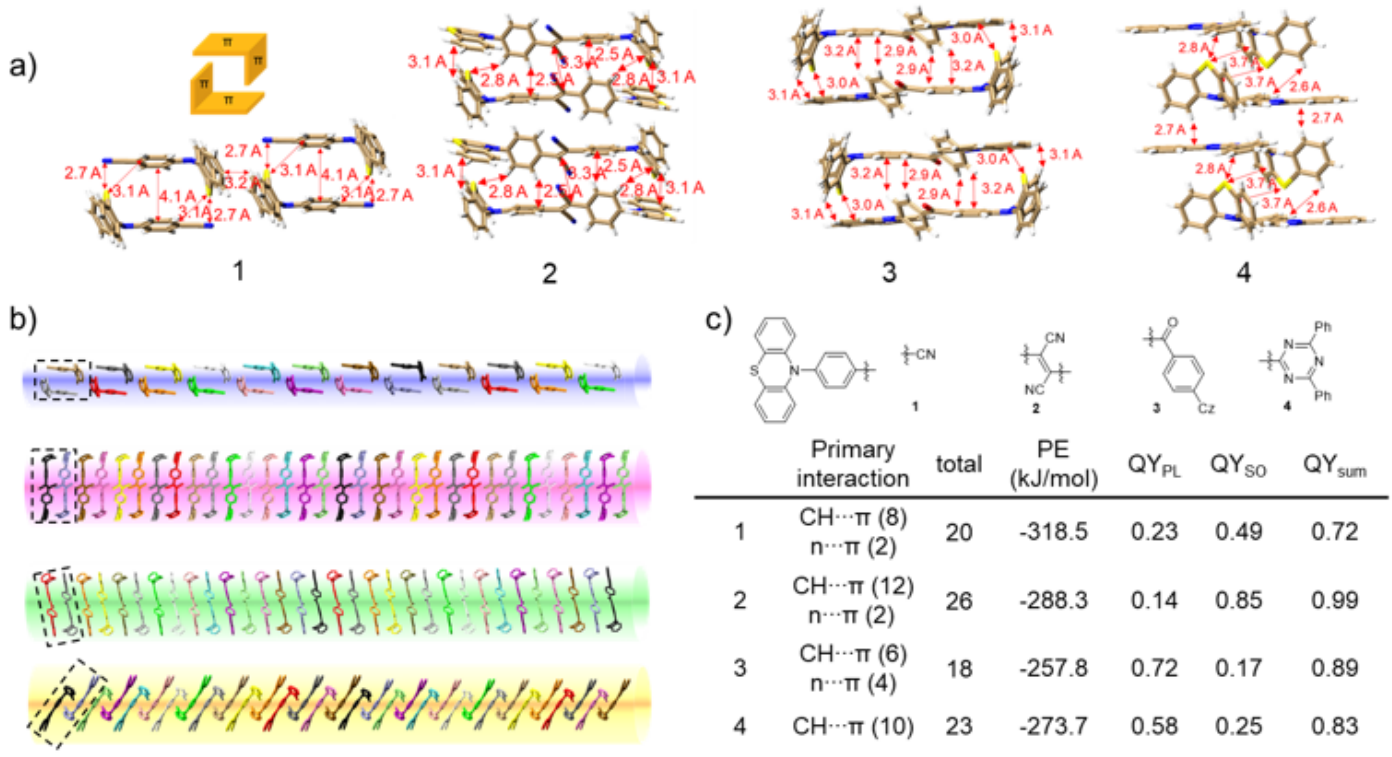

	Primary interaction	total	PE (kJ/mol)	QY_{PL}	QY_{SO}	QY_{sum}
1	CH···π (8) n···π (2)	20	-318.5	0.23	0.49	0.72
2	CH···π (12) n···π (2)	26	-288.3	0.14	0.85	0.99
3	CH···π (6) n···π (4)	18	-257.8	0.72	0.17	0.89
4	CH···π (10)	23	-273.7	0.58	0.25	0.83

Figure 3

Achieving high exciton utilization with 2π molecules. Single-crystal X-ray structures of 1-4. (a) Tubular representations of 1-4. (b) Stacking of molecules (1-4, top to bottom) in 1D molecular column, the colour of column reflects the emission of crystals. (c) Packing feature and exciton utilization (quantum yield) of 1-4: primary interaction in crystalline packing; the total number of short contact (< sum of van-der-Waals radii) per molecule; PE, total packing energy; QYPL, photoluminescence quantum yield; QYSO, single oxygen quantum yield; QYsum, total quantum yield (sum of QYPL and QYSO).

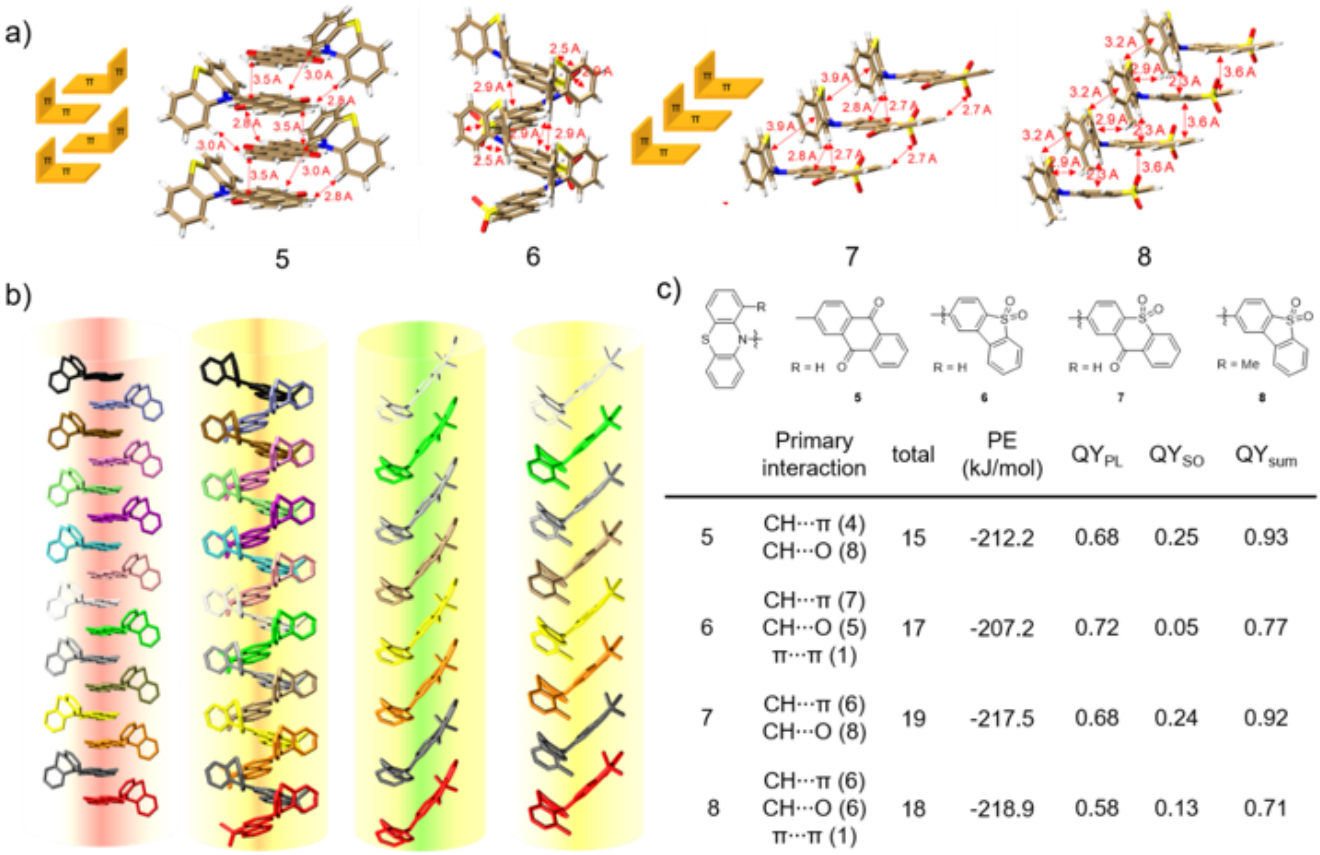

	Primary interaction	total	PE (kJ/mol)	QY_{PL}	QY_{SO}	QY_{sum}
5	CH···π (4) CH···O (8)	15	-212.2	0.68	0.25	0.93
6	CH···π (7) CH···O (5) π···π (1)	17	-207.2	0.72	0.05	0.77
7	CH···π (6) CH···O (8)	19	-217.5	0.68	0.24	0.92
8	CH···π (6) CH···O (6) π···π (1)	18	-218.9	0.58	0.13	0.71

Figure 4

Achieving high exciton utilization with 2π molecules. Single-crystal X-ray structures of 5-8. (a) Tubular representations of 1-4. (b) Stacking of molecules (5-8, top to bottom) in 1D molecular column, the colour of column reflects the emission of crystals. (c) Packing feature and exciton utilization (quantum yield) of 5-8: primary interaction in crystalline packing; the total number of short contact (< sum of van-der-Waals radii) per molecule; PE, total packing energy; QYPL, photoluminescence quantum yield; QYSO, single oxygen quantum yield; QYsum, total quantum yield (add-up of QYPL and QYSO).

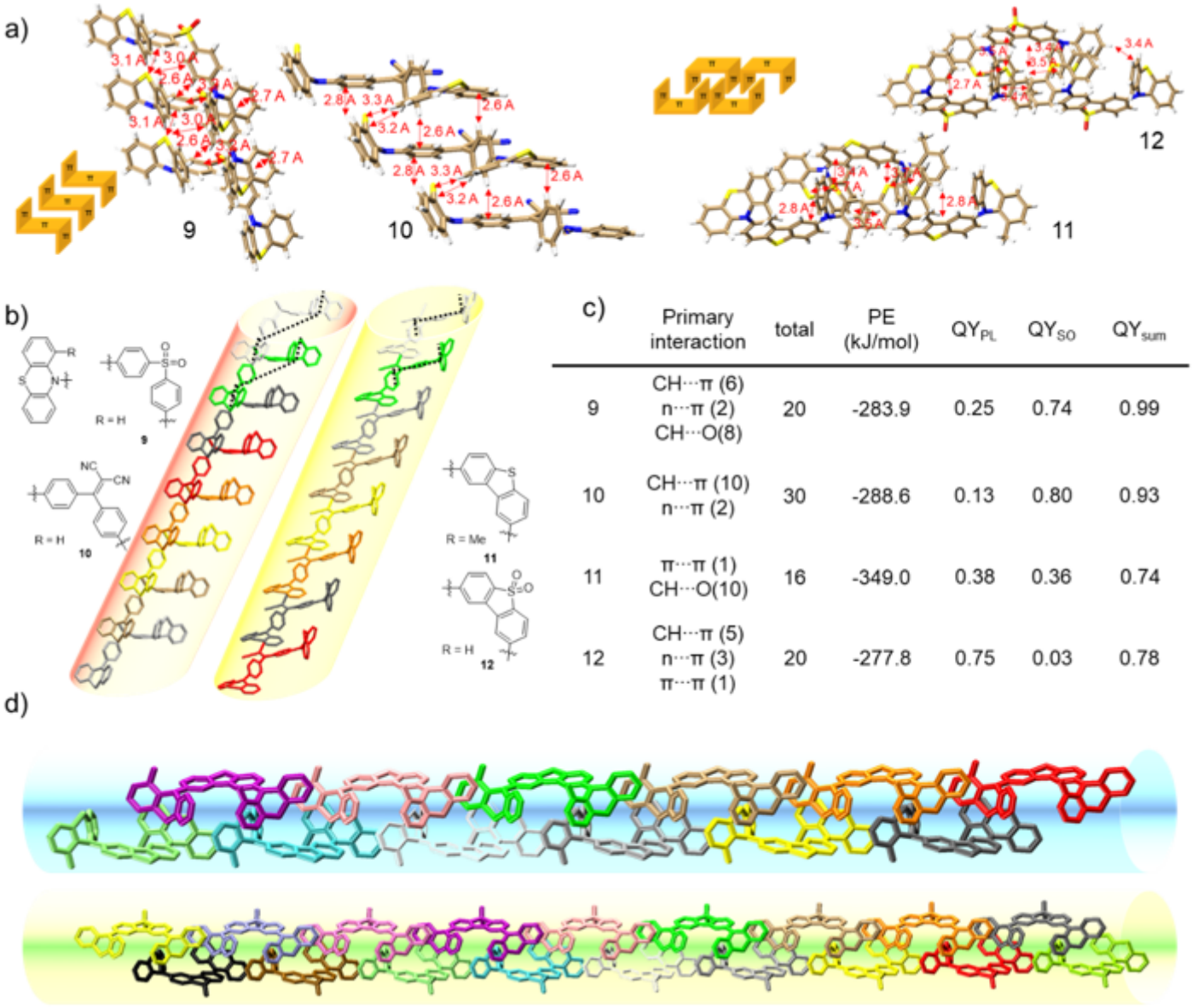

	Primary interaction	total	PE (kJ/mol)	QY_{PL}	QY_{SO}	QY_{sum}
9	CH···π (6) n···π (2) CH···O(8)	20	-283.9	0.25	0.74	0.99
10	CH···π (10) n···π (2)	30	-288.6	0.13	0.80	0.93
11	π···π (1) CH···O(10)	16	-349.0	0.38	0.36	0.74
12	CH···π (5) n···π (3) π···π (1)	20	-277.8	0.75	0.03	0.78

Figure 5

Achieving high exciton utilization with 3π molecules. Single-crystal X-ray structures of 9-12. (a) Tubular representations of 9-12. (b&d) Stacking of molecules in 1D molecular column, the colour of column reflects the emission of crystals. (c) Packing feature and exciton utilization of 9-12: primary interaction in crystalline packing; total refers to the total number of short contacts (< sum of van-der-Waals radii) per molecule; PE, total packing energy; QYsum, total quantum yield.

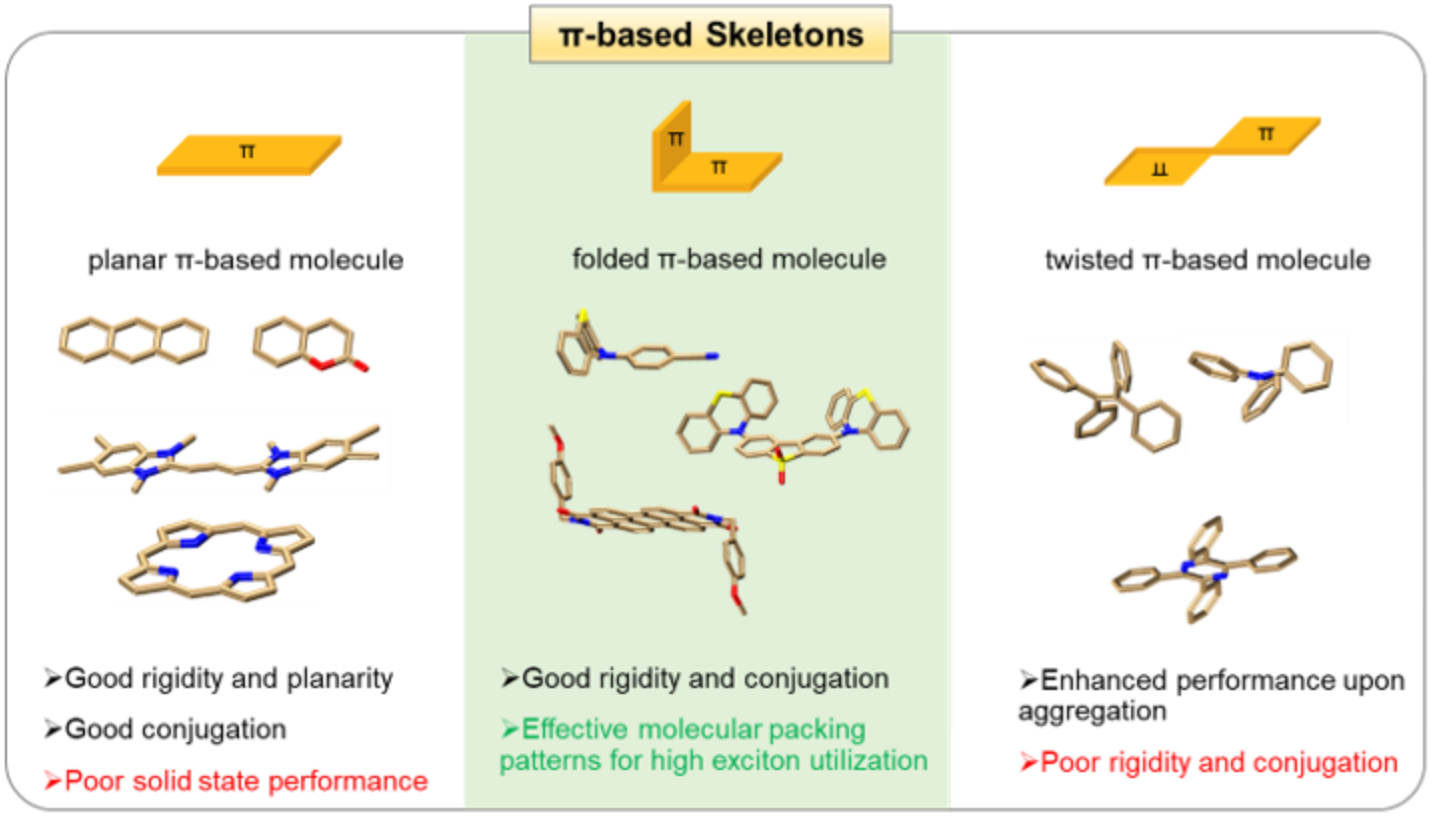

Figure 6

Scheme 1. π-based skeletons. Different π-based skeletons including planar π (e.g. anthracene, coumarin, porphyrin and cyanine), folded π (compounds discussed in this paper) and twisted π (e.g. tetraphenylethene, triphenylamine and tetraphenylpyrazine).

Supplementary Files

This is a list of supplementary files associated with this preprint. Click to download.

- SINCsubmit.docx